Modeling the Fast Gating Mechanism in the ClC-0 Chloride Channel

Mary H. Cheng, Artem B. Mamonov, J. Warren Dukes, and Rob D. Coalson*

Department of Chemistry, University of Pittsburgh, Pittsburgh, Pennsylvania 15260

Received: June 26, 2006; In Final Form: December 5, 2006

A simplified three-dimensional model ClC-0 chloride channel is constructed to couple the permeation of Cl^- ions to the motion of a glutamate side chain that acts as the putative fast gate in the ClC-0 channel. The gate is treated as a single spherical particle attached by a rod to a pivot point. This particle moves in a one-dimensional arc under the influence of a bistable potential, which mimics the isomerization process by which the glutamate side chain moves from an open state (not blocking the channel pore) to a closed state (blocking the channel pore, at a position which also acts as a binding site for Cl^- ions moving through the channel). A dynamic Monte Carlo (DMC) technique is utilized to perform Brownian dynamics simulations to investigate the dependence of the gate closing rate on both internal and external chloride concentration and the gate charge as well. To accelerate the simulation of gate closing to a time scale that can be accommodated with current methodology and computer power, namely, microseconds, parameters that govern the motion of the bare gate (i.e., in the absence of coupling to the permeating ions) are chosen appropriately. Our simulation results are in qualitative agreement with experimental observations and consistent with the "foot-in-the-door" mechanism (Chen et al. *J. Gen. Physiol.* **2003,** *122*, 641; Chen and Miller *J. Gen. Physiol.* **1996,** *108*, 237), although the absolute time scale of gate closing in the real channel is much longer (millisecond time scale). A simple model based on the fractional occupation probability of the Cl^- binding site that is ultimately blocked by the fast gate suggests straightforward scalability of simulation results for the model channel considered herein to experimentally realistic time scales.

1. Introduction

The ClC family of ion channels regulates the flow of Cl^- across cell membranes. By doing so, ClC channels control a variety of important physiological functions, such as skeletal muscle excitability (ClC-1), renal and intravascular transport (ClC-K and ClC-5), and cell volume regulation (ClC-2 and ClC-3). The presence of a double-barreled channel was first suggested by early electrophysiological recordings from the *Torpedo electroplax* ClC-0 channel[1] and was recently confirmed by X-ray crystallography.[2,3] Opening and closing of these two pores appear to be regulated by two distinct mechanisms, corresponding to a fast and a slow gate. Slow gating involves structural changes of both monomers and thus opens or closes both pores simultaneously. The slow gate operates on a time scale of seconds. Fast gating is controlled separately by each individual pore and occurs on a time scale of milliseconds. It was observed experimentally that both gating mechanisms are regulated by Cl^- concentrations.[4−6] Changing the concentrations of Cl^- on the intracellular and extracellular sides of the membrane affects the fast gating in different ways. Increasing the extracellular concentration increases the rate of fast gate opening but has little effect on the closing rate.[5,6] In contrast, increasing the intracellular concentration reduces the rate of fast gate closing but has a much smaller effect on the rate of fast gate opening.[6,7] Thus, it was suggested that the opening and closing of the fast gate are coupled to ion permeation and controlled via two different mechanisms. To explain the dependence of the fast gate closing rate on the internal Cl^- concentration, a "foot-in-the-door" mechanism was proposed,[6,7] according to which a permeating Cl^- ion blocks the fast gate from closing by occupying a binding site that would be occupied by the fast gate in the closed state. Dutzler et al.[2,3] presented a structural basis for this mechanism and suggested that the permeant Cl^- ions compete with the carboxyl group of the E148 side chain for the binding site located closest to the extracellular side. Recently, Accardi and Miller[8] demonstrated that the X-ray crystal structure of EcClC resolved by Dutzler et al.[2,3] was actually an H^+-Cl^- exchange transporter, not a passive ion channel. However, these homologous bacterial ClC protein structures have been successfully utilized to rationalize electrophysiological behavior of several ClC-type ion channels,[3,8,9] and there is strong evidence to support conservation of structure and function among ClC family members.[10−12]

The availability of the crystal structures of bacterial ClC proteins[2,3] has sparked numerous theoretical studies of the Cl^- conduction mechanism as well as that of fast gating in both prokaryotic and eukaryotic pores. Based on an all-atom molecular dynamics (MD) simulation of the StClC channel in a membrane, Cohen and Schulten[13] proposed a king-of the-hill mechanism for Cl^- conduction in which two Cl^- ions compete for an energetically favorable central location in the pore. Using continuum electrostatics calculations and Brownian dynamic (BD) simulations, Corry et al.[14] found that conduction in both ClC-0 and ClC-1 involved three Cl^- ions and was effected by knock-off, similar to that in the KcsA potassium channel[15] and in general agreement with the "king-of-the-hill" mechanism.[13] Bisset et al.[16] used MD simulations combined with Poisson−Boltzmann calculations to study the fast gating mechanism in the ClC-0 channel. They suggested an alternative mechanism to Dutzler et al.,[3] where the fast gate was opened toward the intracellular side by a Cl^- ion coming from the extracellular

* Author to whom correspondence should be addressed. Phone: (412) 624-8261. Fax: (412) 624-8611. E-mail: coalson@pitt.edu

10.1021/jp063993h CCC: $37.00
Published on Web 05/08/2007

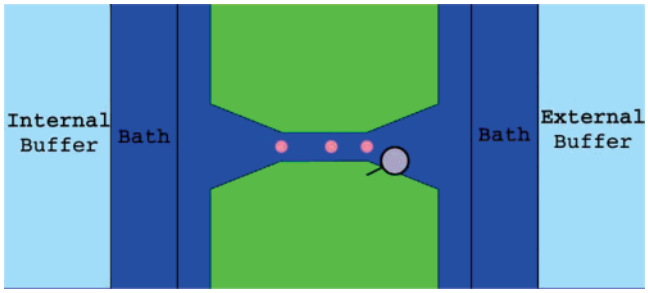

Figure 1. Schematic depiction of the DMC simulation model. The protein/membrane region is shown in green. The gate is represented by a gray particle connected to a pivot rod. Three Cl^- binding sites in the middle of the channel are shown in pink. In each buffer region, a constant number of ions is maintained during DMC simulations. During simulations of the ion motion, the bath concentrations are monitored to assess the performance of the imposed constant concentration boundary conditions.

side. Miloshevsky and Jordan[17] performed a Monte Carlo study on the effect of mutating the charge of some strongly conserved pore-lining residues in prokaryotic transporters. They found that neutralization of E148 as well as mutations of E148 to an uncharged residue (specifically, E148A and E148Q) create an electrostatic well that traps a Cl^- ion in the middle of the pore. The displacement of the trapped Cl^- is enabled by another incoming Cl^- ion, which pushes this trapped Cl^- and promotes anion flow. Bostick and Berkowitz[18] utilized MD simulations to study the effect of protonation of the E148 side chain in StClC and predicted that protonation of the E148 side chain was necessary for the gate to open, in agreement with Miloshevsky and Jordan.[17]

The goal of the present study is to test the foot-in-the-door mechanism proposed for the dependence of the fast gate closing rate on internal and external [Cl^-] using numerical modeling. With currently available computational power, a fully atomistic simulation of ion permeation is intractable on the time scales relevant for studying the fast gating mechanism of ClC channels. Coarse-grained models sacrifice some realism but by virtue of their relative simplicity make it possible to calculate ion permeation kinetics on currently available computing platforms to predict the rate of ion permeation through a variety of open channels. Among such models, Poisson−Nernst−Planck theory,[14,19−21] Brownian dynamics,[14,22−24] and the dynamic Monte Carlo (DMC) technique[25−28] have been extensively applied. However, modeling the gating of ion channels remains challenging because (1) gating often involves large structural changes in the protein channel and (2) gating times far exceed the amount of time that the most powerful computers are able to simulate via MD. To account for this, in the present study we have developed a coarse-grained model that couples the ion permeation to fast gating.

The outline of this paper is as follows. In section 2, we discuss the protocol and rationale for constructing a channel model that mimics ion permeation and the fast (glutamate) gate in ClC channels. We also outline a DMC method for carrying out Brownian dynamics (BD) simulations of ion permeation and the gate motion simultaneously in our model system. In section 3, we discuss our simulation results and present a simple approximate model to accommodate the foot-in-the-door mechanism. Finally, our conclusions are presented in section 4.

2. Methods

2.1. Model Channel. The ClC-0 model channel is depicted schematically in Figure 1; its construction was inspired by

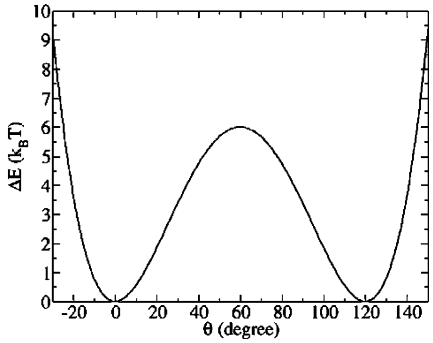

Figure 2. Free energy profile of the fast gate used in our model. $\theta = 0°$ corresponds to the closed state, and $\theta = 120°$ to the open state of the fast gate.

homologous bacterial ClC structures.[2,3] Although the pore of bacterial ClC proteins exhibits significant curvature,[2,3,14] for simplicity we model ClC-0 here as a straight cylindrical pore. The membrane is assumed to be 30 Å wide. The selectivity filter is 12 Å long and 2.5 Å in radius[14] and is connected to two conelike vestibules (abutting the intracellular and extracellular bathing solutions) on either side of the channel. The widest part of these vestibules is 6 Å in radius. Three binding sites for Cl^- ions are asymmetrically located inside the channel at −6, 1, and 6 Å relative to the channel center, approximating the binding sites (S_{int}, S_{cen}, and S_{ext}) in the EcClC selectivity filter postulated on the basis of a recent crystallographic study of one-dimensional anomalous difference electron densities in the selectivity filter at a high Br^- concentration.[29]

Since the fast gate is linked to nonequilibrium chloride permeation through the ClC channel, to model this mechanism the dynamics of the fast gate and permeation of chloride ions must be simultaneously taken into account. In the present study we invoke a minimalist model for the fast gate in which a spherical particle is attached to a lever whose pivot is located in the wall of the pore (cf. Figure 1). The gate particle is allowed to swing from the extracellular vestibule of the channel into the selectivity filter of the channel, thus blocking chloride permeation.

The gate particle has a radius of 2 Å and is meant to mimic the carboxylate moiety of E166 in the ClC-0 channel (the homologous residue to E148 in StClC), which was determined using electrophysiological experiments[3] to be the residue most likely responsible for fast gating in the ClC-0 channel. The pivot of the gate lever was positioned at the (x,y,z) coordinates (−4,0,6), with the z-direction along the channel, the x-direction perpendicular to this, and the origin at the channel center (cf. Figure 1). The length of the lever arm represents the alkyl chain of the glutamate residue and is taken to be 4 Å. The gate particle is assumed to undergo Brownian motion in the symmetric bistable potential shown in Figure 2.

The gate particle coordinate in our model represents the combined motion of dihedral angles $C-C_\alpha-C_\beta-C_\gamma$ and $C_\alpha-C_\beta-C_\gamma-C_\delta$ of the E166 side chain. We inferred the relevance of these dihedral angles by studying the homologous E148 residue in crystal structures of bacterial ClC pores.[2,3] Root-mean-square deviation alignment of the closed pore structure (PDB code 1KPL) with the putative open structure (PDB code 1OTU) showed that they are very similar except that the closed pore is obstructed by the E148 side chain. Furthermore, we compared internal degrees of freedom of the E148 side chain in the open and closed structures and found that dihedral angles $C-C_\alpha-C_\beta-C_\gamma$ and $C_\alpha-C_\beta-C_\gamma-C_\delta$ contribute the most to the difference in the two structures, namely, the dihedral angle $C-C_\alpha-C_\beta-C_\gamma$ is different by ca. 90° and the dihedral angle

TABLE 1: Parameters Used in Our DMC Simulations[a]

	set 4.6	set 6	set 6.7	set 8
E_{act}, k_BT	4.6	6	6.7	8
D_{gate}, Å^2/ps	0.02	0.061	0.02	0.061
k_{esc}, ns^{-1}	0.04732	0.04633	0.008424	0.008377

[a] Rate constants were calculated using eq 10.

$C_\alpha-C_\beta-C_\gamma-C_\delta$ is different by ca. 4°. To keep our model simple we have chosen to map both of these angles into one effective gate coordinate described by angle θ, such that $\theta = 0°$ corresponds to the closed conformation and $\theta = 120°$ to the open one. We increased the open angle to slightly larger than 90° so that in the putative open state the lever of the gate runs roughly parallel to the conelike vestibule. The wells of our bistable potential correspond to stable states (i.e., the gate in the open or closed state) where the E148 side chain in bacterial ClC forms hydrogen bonds with neighboring residues and is in favorable electrostatic interaction with the surrounding medium, (i.e., bridging the helices αF and αN together through hydrogen bonding in the gate closed conformation[3,18] or forming a salt bridge with R147[18,30] in the gate open configuration). The barrier corresponds to configurations lacking hydrogen bonds. On the basis of the observations above, the effective bistable potential energy function for the gate was taken as $\phi_g(\theta) = E_{act}((\theta - 60)^2 - 60^2)^2/60^4$, where θ is the angle of the gate lever and E_{act} is the height of the energy barrier. The closed state of the gate corresponds to the angle $\theta = 0°$. In this state the gate lever is perpendicular to the channel (z) axis. The open state of the gate is located at $\theta = 120°$. The maximum barrier height of the gate is at $\theta = 60°$. In our computational study we employed several sets of gate parameters, which are reported in Table 1. The choice of parameters is discussed at length below.

The radii of mobile Cl^- and Na^+ ions were taken to be 1.8 and 1 Å, respectively. Inside the channel these ions move in the presence of the single ion potential of mean force (PMF) profiles shown in Figure 3 together with electrostatic interactions from other ions or the gate particle (i.e., negatively charged E166) and any additional electric potential applied across the membrane (e.g., via microelectrode techniques). The Cl^- PMF has three energy wells, which mimic experimentally determined Cl^- binding sites in EcClC.[3,29] In the current literature, there is no consensus as to the binding free energy of Cl^- ions to the S_{int}, S_{cen}, and S_{ext} binding sites.[17,18,30,31] PMF profiles predicted by MD simulations[13,18] may not be appropriate for direct input into a coarse-grained model due to uncertainties in the underlying MD force fields (e.g., the approximate treatment of electronic polarizability). Furthermore, coarse-grained prediction of the PMF profile, e.g., via Poisson−Boltzmann calculations,[31] is highly dependent on methodological uncertainties (i.e., the protein dielectric constant and protonation states of ionizable residues). So, in the present study, we followed a procedure employed in ref 32 to estimate the single ion PMF in the ClC-0 channel. The well depths and barrier heights of the Cl^- PMF were adjusted to reproduce a saturation behavior of the gate open time with internal [Cl^-] and a current−concentration profile similar to that in ClC-0 (vide infra). The energy barrier for Na^+ permeation was chosen to be $35k_BT$, similar in magnitude to that invoked in a previous ClC-0 model channel.[14] Such a high-energy barrier excludes the permeation of Na^+ ion through the ClC-0 model channel, consistent with an MD investigation of Na^+ transport in the StClC pore.[18] The diffusion coefficient for both Na^+ and Cl^- was set to 0.2 Å^2/ps in the bulk[33] and assumed to be linearly reduced from this bulk value at the channel entrances ($z_L = -20$ Å and $z_R = 20$ Å) to a value 10 times smaller than the bulk value at the selectivity filter entrance ($z_L = -14$ Å and $z_R = 14$ Å) and then maintained at the smaller value (i.e., 0.02 Å^2/ps) throughout the transmembrane domain -14 Å $< z <$ 14 Å. Such a small diffusion coefficient for ions inside the ClC-0 channel was chosen based on our previous studies of the K^+ diffusion coefficient in the gramicidin A channel, where reduction of ca. 10 times compared to that in bulk water was found.[34] Since the pores of the ClC channels are very narrow[14,18] and Cl^- ion is partially dehydrated by the side chains lining the pore and is coordinated not only by side chains but also by backbone atoms,[13] a similar large reduction of the ion diffusion coefficient is expected.

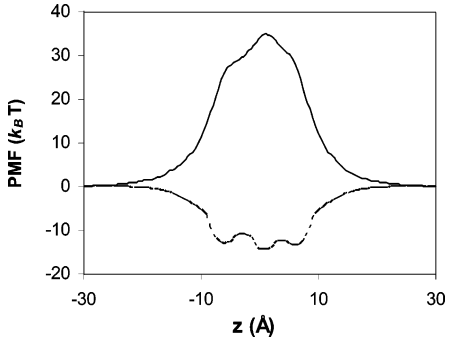

Figure 3. One-dimensional PMF for a single Na^+ (solid line) or Cl^- (dashed line) for transport through an empty channel with neutralized E166 in the absence of external potential. Following a procedure described in ref 32, the Cl^- PMF was estimated by adjusting the well depths and barriers of the free energy profile associated with the binding sites reported in ref 29 to generate a saturation behavior of the gate open time with internal [Cl^-] and a saturated current−concentration behavior found in the ClC-0 channel. A high-energy barrier was assumed for Na^+, following the treatment given in ref 14.

2.2. Dynamic Monte Carlo Method. We used a dynamic Monte Carlo (DMC) method to simulate ion permeation and motion of the gate simultaneously. Complete computational details of our DMC algorithm and its application to ion permeation through protein channels can be found in refs 25−28. Here we will give a brief summary of the computational model and method.

In our DMC algorithm for ion permeation,[25−28] configurations are generated by random changes of the ion positions. The total number of ions is characterized by $N = N_L + N_R + N_I + N_v$. Here N_L and N_R are the fixed numbers of ions on the left and right boundaries (buffer regions in Figure 1), which are obtained by integrating the given boundary concentrations C_L and C_R over the volumes of the boundary layers. In the present study, constant concentration boundary conditions are imposed by randomly distributing N_L or N_R ions in the buffer regions at each Monte Carlo (MC) cycle. N_I is the number of ions inside the system, and N_v is the number of virtual ions. The total number of ions N is fixed, and N_I fluctuates. N_v is introduced only for counting purposes and is included to account for dynamic fluctuation of the number of ions in the interior of the system and to ensure the proportionality of Monte Carlo cycles to real time.[26] For example, in the DMC simulation that involved the ionic concentration of 0.135 M NaCl on both sides of the membrane (see section 3 for full details), the number of ions in the left buffer was the same as in the right, namely, $N_L = N_R = 4$ (2 for Cl^- and 2 for Na^+ to make the buffer neutral), the number of ions in the internal system was $N_I = 8$, and the virtual number of ions was taken as $N_v = 2$; thus the total number of ions used was $N = 18$.

One MC cycle consists of N steps. At each step, one ion k is randomly chosen to move $\pm h$ in one direction (x, y, or z) if the

chosen ion is not a virtual one, where h is a position-dependent displacement, as detailed below. In the present implementation, this new configuration is accepted if Rand < $\exp(-\beta\Delta W)$, where Rand is a uniform random number on the interval [0,1] and $\beta = (k_B T)^{-1}$; ΔW is the energy change between the old and the new configurations based on the chosen ion k with charge q_k. In the present study, ΔW is calculated as[27]

$$\Delta W = W_k^{\text{new}} - W_k^{\text{old}} \tag{1}$$

$$W_k = \phi_k^{\text{stat}} + \sum_{j\neq k} \frac{q_k q_j}{\epsilon_w} \phi^{\text{Coul}}(r_{kj}) + \sum_{j\neq k} q_k q_j \phi_{kj}^{\text{diel}} + \frac{q_k q_g}{\epsilon_w} \phi^{\text{Coul}}(r_{kg}) + q_k q_g \phi_{kg}^{\text{diel}} - k_B T \ln(D(z)/D_0) \tag{2}$$

where q_j and q_g are the charges of ion j and the gate particle, respectively. Furthermore, D_0 and $D(z)$ are the diffusion constants of an ion in the bulk and at position z, respectively. The first term on the right-hand side of eq 2 is the single ion free energy corresponding to transport through an empty channel with a neutralized E166 residue. In the present study, we calculated this single ion free energy by superimposing the single-particle PMF (cf. Figure 3) of ion k with the applied external potential field calculated by solving Poisson's equation in the dielectric profile defined in Figure 1. The second term represents Coulombic interactions between pairs of ions in a dielectrically uniform environment characterized by the water dielectric constant ϵ_w, and the third term corresponds to the "image" potential experienced by ion k due to the surface charge induced by ion j. The fourth term corresponds to Coulombic interactions between the gate particle and the chosen ion k in a dielectrically uniform environment, and the fifth term contributes to the image potential experienced by ion k due to the surface charge induced by the gate particle. The effects of the dielectric inhomogeneity of the channel environment on the ion−ion and ion−gate electrostatic interactions (the third and fifth terms in eq 2) were implemented using an efficient empirical pair potential[25]

$$\phi_{kj}^{\text{diel}} = 2\sqrt{\phi_{k\leftarrow k}^{\text{diel}}\, \phi_{j\leftarrow j}^{\text{diel}}} \exp(-c r_{kj}/L) \tag{3}$$

where $\phi_{k\leftarrow k}^{\text{diel}}$ and $\phi_{j\leftarrow j}^{\text{diel}}$ are the dielectric contribution to the self-energy (or the image potential) for ions k and j with a unit (proton) charge. Since the model channel is very narrow, the dielectric contribution to the self-energy is further simplified and calculated as a one-dimensional (z) function along the channel center line. A detailed description for calculating $\phi_{k\leftarrow k}^{\text{diel}}$ can be found in ref 25. L is the length of the channel, r_{kj} is the distance between the ions k and j, and $c = 2.0$. We take the dielectric constant in the water bath ϵ_w to be the same as that inside the channel, namely, $\epsilon_w = 80$ in all aqueous regions. Unless otherwise specified explicitly, for the entire protein−membrane system, a uniform dielectric constant of $\epsilon_p = 20$ is used, which falls within the range of previously adopted protein dielectric constants.[35−37]

Finally, the last term in eq 2 is included to account for the effect of the nonuniform ion diffusion constant profile, which in the model considered in this paper varies only along the channel direction. The diffusion constants and the associated ion displacements taken in one DMC step obey the relation

$$h_z^2/D(z) = h_0^2/D_0 \tag{4}$$

where h_0 and h_z are the associated ion displacement in the bulk and at position z, respectively. The total simulation time T_s for ions is related to the number of the Monte Carlo cycles N_c as

$$T_s = \frac{h_0^2 N_c}{6D_0} \tag{5}$$

The gate particle is assumed to undergo one-dimensional Brownian motion along the angular coordinate. In one MC step, the gate attempts to move through an angle $\pm\Delta$. This new configuration is accepted if Rand < $\exp(-\beta\Delta W_g)$, where ΔW_g is the energy change of the gate particle between these two configurations. The energy of the gate is calculated as follows

$$W_g = \phi_g(\theta) + \sum_j \frac{q_g q_j}{\epsilon_w} \phi^{\text{Coul}}(r_{gj}) + \sum_j q_g q_j \phi_{gj}^{\text{diel}} \tag{6}$$

where $\phi_g(\theta)$ is the angle-dependent intrinsic gate potential energy (cf. Figure 2). The second term represents the Coulombic interactions between the gate particle and the ions, again, assuming an uniform dielectric constant ϵ_w, and the third term corresponds to the image potential experienced by the gate particle due to the surface charge induced by ion j. The total simulation time for the gate particle T_g is related to the number of Monte Carlo cycles N_g for the gate particle (each gate particle cycle consists of one attempted gate particle move) according to

$$T_g = \frac{(L_g\Delta)^2 N_g}{2D_{\text{gate}}} \tag{7}$$

where L_g is the length of the gate arm and D_{gate} is the diffusivity of the gate. To synchronize time between the gate particle and the mobile ions, the angular displacement of the gate is related to the ion displacement in the bulk as follows

$$(L_g\Delta)^2/D_{\text{gate}} = h_0^2/3D_0 \tag{8}$$

Note that in our DMC method for simulating ion permeation and motion of the gate, a hard-core excluded volume potential is also included. In particular, we do not permit overlap between an ion and the protein/membrane, between any two ions, or between ions and the gate particle. If an attempted move gives rise to this type of overlap, it is rejected.

The computational box (excluding the buffer region) has a size of $L_x \times L_y \times L_z = 40 \times 40 \times 60$ Å^3 . Unless otherwise explicitly noted, the displacement of ions in the bulk was set to 1.0 Å for all simulation parameter sets, and a −100 mV external electric potential was applied across the membrane. The gate open time was calculated as the time it took for the gate, initially positioned in the open state (corresponding to $\theta = 120°$) to close (i.e., reach $\theta = 0°$) for the first time.

3. Results and Discussion

3.1. Test of the Gate Motion Using a Simple Analytical Model. To test our DMC algorithm for simulating combined ion permeation/gate particle motion, we first considered one-dimensional motion of the gate particle according to the potential $\phi_g(\theta)$ in the absence of any coupling to ion permeation; i.e., the channel was empty of ions. Simulation results for the escape rate (rate of transitions from the initial to the final state well,

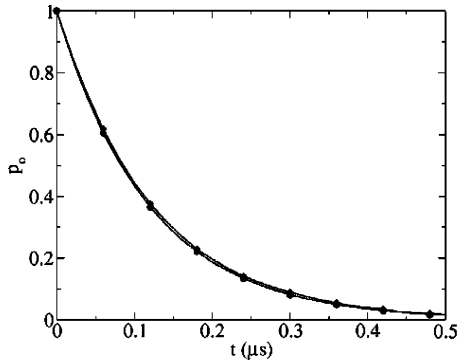

Figure 4. Probability that the neutral gate is open at time t for parameter set 6 (cf. Table 1) calculated using Kramer's rate theory (circles) and DMC (diamonds). The error bars for DMC data are smaller than the symbol labels.

suppressing any back transitions from the final to the initial state well) were compared to the corresponding predictions of Kramer's theory in the high friction limit, namely[38]

$$k_{esc} = \frac{\omega_w \omega_b}{2\pi\xi} e^{-E_{act}/k_B T} \quad (9)$$

where k_{esc} is Kramer's escape rate constant, E_{act} is the height of the energy barrier (activation energy), and ξ is the coefficient of dynamical friction of the escaping particle. Furthermore, ω_w and ω_b are harmonic curvatures describing the potential energy well and the escape barrier, respectively. Specifically, $\omega_w = \sqrt{k_w/m}$, where m is the particle mass and $k_w > 0$ is the second derivative of the gate particle potential function evaluated at the bottom of the reactant well; analogously, $\omega_b = \sqrt{k_b/m}$ with $k_b > 0$ being the negative of the second derivative of the gate particle potential evaluated at the top of the barrier. Through the use of Einstein's relation $D = k_B T/m\xi$, eq 9 becomes

$$k_{esc} = \frac{D_{gate}\sqrt{k_w k_b}}{2\pi k_B T} e^{-E_{act}/k_B T} \quad (10)$$

where D_{gate} is the diffusion constant of the gate particle. Note that the mass of the particle does not appear in eq 10 since it is incorporated into the diffusion constant. Transition of the gate particle from the open to the closed state is analogous to a first-order chemical reaction, where the open state corresponds to the reactant and the closed state to the product. Therefore, the probability for the gate to remain open at time t is[39]

$$p_o(t) = e^{-k_{esc} t} \quad (11)$$

Table 1 lists several sets of D_{gate}, E_{act}, and the calculated k_{esc}. (These values of D_{gate} and E_{act} were chosen for reasons outlined below in section 3.3.) We calculate $p_o(t)$ analytically via eqs 10 and 11 and then compare to the corresponding numerical calculation results obtained using the DMC method, as illustrated in Figure 4. Excellent agreement is found.

3.2. Dependence of the Gate Open Time on Internal and External [Cl⁻]. In several ClC-type channels, the current is observed to increase with the bath Cl^- concentration and then saturates to a maximum value following the Michaelis−Menten form $I = I_{max}/(1 + Cl_s/[Cl])$,[14] where I_{max} is the saturation current and Cl_s is the concentration at which half of the saturation current is attained. A comparison of the current−concentration relationship obtained in our model channel with experimental study is shown in Figure 5. Numerical simulations were carried

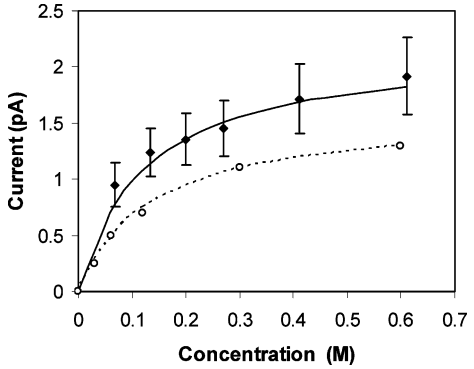

Figure 5. Comparison of current−concentration relationship for the ClC-0 channel. Both experiment and simulations were carried out with symmetric bathing solutions. Filled diamonds with error bars represent simulation results, and the experimental measurements taken from ref 14 are shown by open circles. The data points are fit by solid line (simulation results) and dashed line (experimental data) using the Michaelis−Menten equation.

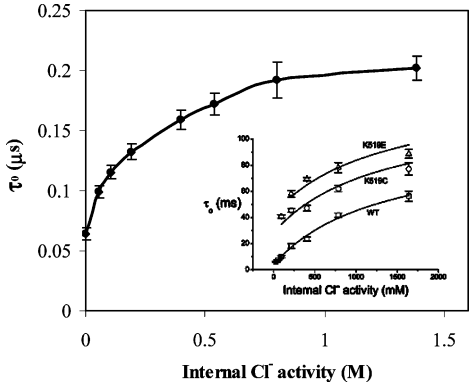

Figure 6. Dependence of the gate open time on internal Cl^- activity for the neutral gate and parameter set 6 (cf. Table 1) calculated using DMC. External $[Cl^-]$ was kept constant at 0.135 M. Each simulation data point represents the average of 500−1000 separate runs. Error bars were estimated based on the average over a set of 100 runs. The Cl^- activity $a_{Cl} = \mu[Cl^-]$ was calculated using the activity coefficients μ given in ref 46. Corresponding experimental measurements[7] are shown in the figure inset.

out in symmetric bathing solutions and an applied external potential of −80 mV for ∼3.3 μs. During these simulations, the gate was taken to be neutral and restrained in its open state ($\theta = 120°$). The half saturation points determined from our model channel and experimental measurements are 125 and 136 mM,[14] respectively. Our saturation current is 2.2 pA, which is somewhat larger than the experimental value of 1.6 pA. Overall, our model ClC-0 channel generates a current−concentration relationship in respectable agreement with the experimentally observed curve.

To computationally validate the foot-in-the-door mechanism for the ClC channel, we studied two basic relationships that were measured experimentally,[6,7] namely, (i) the dependence of the gate open time on internal $[Cl^-]$ while keeping external $[Cl^-]$ constant at 0.135 M and (ii) the dependence of the gate open time on external $[Cl^-]$ while keeping internal $[Cl^-]$ constant at 0.135 M. Results of the open time dependence on internal $[Cl^-]$ for parameter set 6 (cf. Table 1) are shown in Figure 6 for the case of a neutral gate. (Analogous results for a gate with −1 charge, representing the deprotonated state of E166, are presented in section 3.5.) To scan the range of $[Cl^-]$ used in experiments,[6,7] the following set of constant concentrations was imposed in the internal buffer region (cf. Figure 1): 0.0675, 0.135, 0.270, 0.54, 0.81, 1.22, and 2.02 M. The average

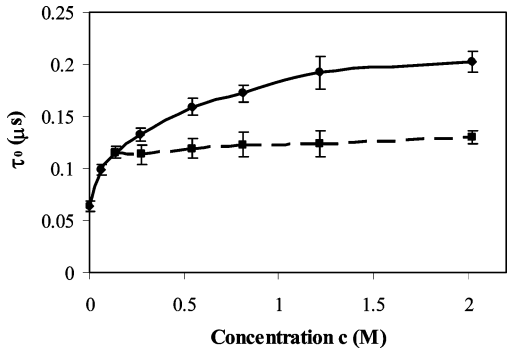

Figure 7. Dependence of the gate open time on external [Cl^-] (squares with error bars) for a neutral gate with parameter set 6 (cf. Table 1) calculated using DMC. Internal [Cl^-] was kept constant at 0.135 M. For comparison, dependence of the gate open time on the internal [Cl^-] is also shown (circles with error bars).

bath concentrations (cf. Figure 1) were found to fluctuate within 5% of the specified concentrations as 0.0657 ± 0.0038, 0.1283 ± 0.005, 0.2536 ± 0.006, 0.5147 ± 0.008, 0.7781 ± 0.009, 1.194 ± 0.011, and 2.044 ± 0.013 M, indicating successful implementation of constant concentration boundary conditions in our simulation system. A monotonic saturation of the open time is observed when the internal [Cl^-] is increased from 0 to 2 M, which is in qualitative agreement with experimental observations[7] shown in the inset of Figure 6. This saturation behavior observed in our simulations is consistent with the foot-in-the-door mechanism proposed by Chen and Miller.[7] At low [Cl^-], the probability of the S_{ext} site, i.e., the Cl^- ion binding site closest to the extracellular side, being occupied by a Cl^- ion (thus preventing the gate from closing) increases linearly with internal [Cl^-] since the flux through the channel scales linearly with internal bathing solution concentration at low concentration (cf. Figure 5). At higher concentrations, S_{ext} becomes "clogged" with Cl^-, and further increase of the internal bath concentration of Cl^- does not significantly increase the probability that S_{ext} will be occupied by Cl^-. Thus a saturated gate open time is observed. (Further discussion of this point is provided in section 3.4.)

Results of DMC calculations for the dependence of gate open time on external [Cl^-] are shown in Figure 7. Our simulations show a relatively weak dependence of gate open time on the external [Cl^-], qualitatively consistent with experimental measurements.[6,7] Such behavior might be expected in the model channel explored here, since the Cl^- ions are being driven from the internal to the external side by the applied membrane potential and thus should be less sensitive to the ion concentration in the external compartment. The dependence of gate open time on the external [Cl^-] was not further investigated because of the speculated presence of a fourth binding site on the extracellular side whose existence could significantly affect how extracellular Cl^- ions regulate opening and closing of the gate.[9,18,40] The location of the fourth binding site has not yet been experimentally identified, and therefore, the fourth binding site was not included in our model.

3.3. Effects of D_{gate} and E_{act}. Figure 6 illustrates the qualitative agreement between our numerical simulations and experiments. However, the absolute values of our calculated gate open times are more than 5 orders of magnitude smaller than the experimentally measured ones. In reality, the gate open time for the fast gate of the ClC channel is in the multi-millisecond time scale, well beyond the time scale that can be computationally accessed at present. (Recall that in three-dimensional Brownian dynamics or DMC simulations of ion channel permeation kinetics, data are typically collected for several microseconds.) Our model is crude of necessity: There are no experimental measurements of the gate diffusion constant in the ClC channel, and the magnitude of the activation energy for the fast gate is not known either. Therefore, we have treated them as adjustable input parameters for our DMC calculations and have chosen these gate parameters (i.e., D_{gate} and E_{act}) so as to accelerate the simulation of gate closing to a time scale that can be accommodated with current computer power. We used four sets of D_{gate} and E_{act} parameters in our DMC simulations (Table 1). These parameters were selected to study the combined influence of D_{gate} and E_{act} according to the value of k_{esc} to which they correspond. Two different values of D_{gate} were considered, 0.061 and 0.02 $Å^2$/ps, i.e., 3 and 10 times smaller, respectively, than the ion diffusion constant in bulk water, and thus on the same order of magnitude as the ion diffusion constant inside the channel. Clearly, the gate diffusion constants employed in this study serve as very crude estimates of the diffusion constant of the E166 (homologous to E148 in StClC) side chain responsible for the fast gating in our model. Fortunately, our numerical calculations (discussed below) reveal that the essential saturation behavior of the gate open time does not depend in an essential manner on the value of D_{gate}.

Four different values of E_{act} were selected: $4.6k_BT$, $6k_BT$, $6.7k_BT$, and $8\ k_BT$. This range of activation energies was chosen to satisfy the lower limit of applicability of Kramer's theory (ca. 1 k_BT) and at the same time lead to barrier crossing (in our case, gate closing) within reasonable computation time. (The barrier crossing time goes up exponentially with E_{act}.) The parameters D_{gate} and E_{act} were selected such that sets 4.6 and 6 had a similar k_{esc} and sets 6.7 and 8 had a similar k_{esc}, roughly 5 times smaller than that corresponding to sets 4.6 and 6 (Table 1).

Results of the dependence of gate open time on internal [Cl^-] for parameter sets 4.6 and 6 are shown in Figure 8a. Figure 8b shows the result for parameter sets 6.7 and 8. All sets of simulations were performed using a neutral gate. Saturation behavior is observed for all parameter sets. On the basis of these results we can conclude that saturation behavior of the gate does not depend significantly on D_{gate} and E_{act} individually but only on their combined influence on k_{esc}.

We also compared the saturation behavior of the gate open time on internal [Cl^-] for parameter sets corresponding to significantly different values of k_{esc} (cf. Table 1). For the sake of comparison we normalized the gate open time for all parameter sets by dividing the open time by that at internal [Cl^-] = 0 and plotted them on the same graph (cf. Figure 9). All four sets predict nearly identical saturation behavior. This result implies that k_{esc} simply scales the curve of the gate open time but that the curve shape is determined by some "universal" mechanism. In fact, this mechanism relies on saturation of the fractional occupation probability of the external binding site (S_{ext}) with Cl^- as the internal [Cl^-] increases, as discussed in detail in section 3.4 below. An important corollary of this observation is that if k_{esc} was much slower (comparable to the experimentally measured values), then we would expect the same normalized curve for the gate open time, and therefore our model would be able to account semiquantitatively for the experimentally measured saturation of the gate open time with internal [Cl^-]. To illustrate this feature, we also compare our DMC simulation results in Figure 9 with appropriately normalized gate open times for the K519C ClC-0 channel. In particular, the experimentally measured open times were divided by a factor of 25 ms. (Thus, the gate open time value for [Cl^-] = 0, i.e., $\tau_{o,0}$, is ca. 25 ms.) The correspondence between experimental

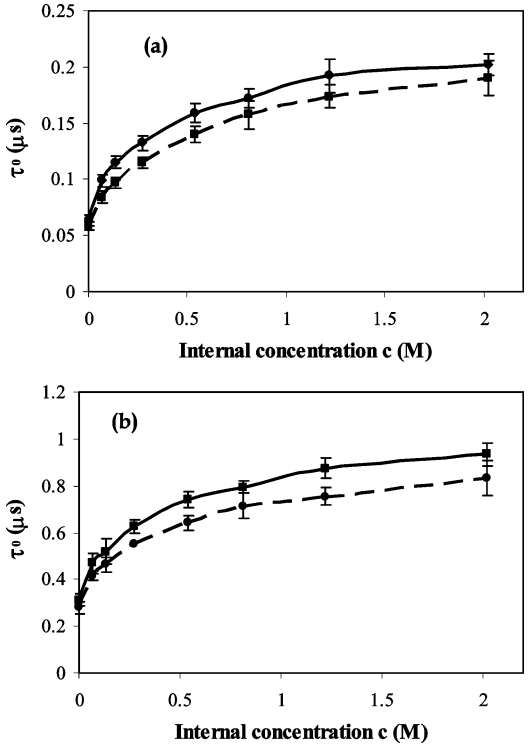

Figure 8. Dependence of the gate open time on internal [Cl^-] for a neutral gate calculated via DMC. (a) Results for parameter set 6 (circles with solid line) are compared with results for parameter set 4.6 (squares with dashed line). (b) Results for parameter set 6.7 (circles with dashed line) are compared with results for parameter set 8 (squares with solid line). See Table 1 for parameter values.

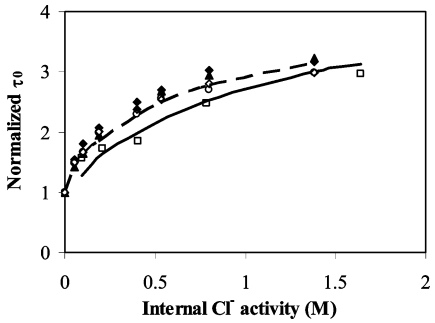

Figure 9. Comparison of the dependence of the normalized neutral gate open time on internal Cl^- activity. The open time was normalized by dividing it by the open time at internal [Cl^-] = 0. Results for parameter set 4.6 (filled diamonds), set 6.0 (filled triangles), set 6.7 (open circles), and set 8.0 (open diamonds) are compared with the normalized gate open time obtained experimentally in the K519C ClC-0 channel[7] (open squares). The gate open time in K519C was normalized to the value of 25 ms. Dashed and solid lines represent a curve fitting of simulation results and experimental data, respectively.

and computational results is rather good. While we do not claim that a universal scaling law of this type exists at a quantitative level for all experimental conditions and channel compositions, such behavior does obtain qualitatively for a wide range of experimental examples.

3.4. Approximate Factorization of the Gate Closure Mechanism. The saturation behavior of gate open time with internal [Cl^-] concentration implies that as the internal [Cl^-] concentration increases the S_{ext} site of the channel pore is more likely to be occupied at any particular time by a Cl^- ion, thus preventing the gate from occupying the same site, i.e., closing. This is the qualitative essence of the foot-in-the-door mechanism. Saturation of the gate open time is then expected to correlate directly with saturation of the occupation probability (i.e., fractional occupation time) of the S_{ext} site by Cl^- ions, which is anticipated on the basis of chemical kinetics principles when there is an intermediate state that becomes maximally occupied as more and more particles attempt to traverse the reaction pathway.[39] To quantify these ideas in the context of the present model of coupled gate particle/ion motion, we can think of the "bare" escape rate along the one-dimensional reaction coordinate traversed by the gate particle as providing the rate of successful traversal of the reaction barrier. For a one-dimensional barrier crossing process, any particle starting in the reactant state that makes it over the barrier is captured in the product state (assuming that the product well is replaced by a probability sink), corresponding in our system to a gate closing event. However, in the full many-body model under investigation here, in which gate closing is coupled to ion permeation through the channel pore, some of the barrier crossing events described above are blocked by the presence of a Cl^- ion in the product well region. This causes the observed closing rate to be reduced from the value given by Kramer's escape rate constant, roughly by a factor of $(1 - f_{S_{ext}}(c))$, where $f_{S_{ext}}(c)$ is the probability that the S_{ext} site is occupied by a Cl^- ion, which is in turn a function of the internal chloride concentration $c = [Cl^-]_{int}$. With increasing c, $f_{S_{ext}}(c)$ saturates to a maximum value less than unity, and thus the observed gate closing rate saturates to a corresponding minimum value. Furthermore, it seems reasonable to expect that the function $f_{S_{ext}}(c)$ will be largely independent of the dynamics of the gate particle in its open state since fast gating is thought to be controlled by a local conformation change[3] and the time scale for the gate to close is much longer than that for ion permeation: thus, a steady-state ion occupation probability inside the channel can be assumed. If all of the elements of the scenario just outlined are valid, then the exact values of the activation barrier and diffusion constants of the reaction coordinate for the gate particle are not critical for describing the dependence of gate closing time on internal [Cl^-], in the sense that this curve scales proportionally to Kramer's k_{esc} and the scaling of k_{esc} with details of the gate particle reaction coordinate is well-understood (cf. eq 10).

To examine the validity of this mechanism factorization, we carried out appropriate numerical simulation studies on our model system and compared results of gate open time calculated using the DMC method with those implied by the simple factorized mechanism. The latter implies that the gate open time is related to occupation probability of Cl^- in the external binding site according to

$$\tau_o(c) = \tau_{o,0}/(1 - f_{S_{ext}}(c)) \qquad (12)$$

where $\tau_{o,0}$ is the average gate open time without Cl^- in the system extracted from DMC simulations. (As indicated in section 3.1, the value of $\tau_{o,0}$ is well-approximated (typically to within ca. 25%) by k_{esc}^{-1}, where k_{esc} is the one-dimensional Kramer's escape rate constant in eq 10.) In practice, $f_{S_{ext}}(c)$ was calculated by monitoring the fraction of time steps in the DMC simulation (before the gate closed) at which a Cl^- ion occupied a z position in the range $|z_{Cl^-} - z_{S_{ext}}| \leq R_{gate}$ where z_{Cl^-} is the z coordinate of the Cl^- center, $z_{S_{ext}}$ is the z coordinate of the center of the external binding site, and R_{gate} is the radius of the gate particle. $f_{S_{ext}}(c)$ was found to be nearly saturated to a maximum value of 0.81 at internal [Cl^-] = 2.02 M. The dependence of the ion density inside the channel system on internal [Cl^-] is shown in Figure 10. [Note: The ion density $\langle n_{cl} \rangle$ inside the channel was determined by the following

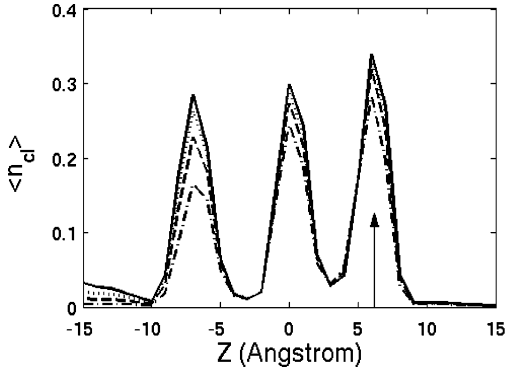

Figure 10. The average number density of Cl^- ions (number of ions/Å) along the channel axis at steady state for several different internal Cl^- concentrations calculated via DMC for parameter Set 6.7 (Table 1). The internal [Cl^-] was set to 0.135 M (dash-dotted line), 0.54 M (dashed line), 1.22 M (dotted line) and 2.02 M (solid line). The location of the external binding site S_{ext} is indicated by an arrow. The same external electric potential of −100 mV was used for calculations at all concentrations. Similar profiles were observed using other parameter sets.

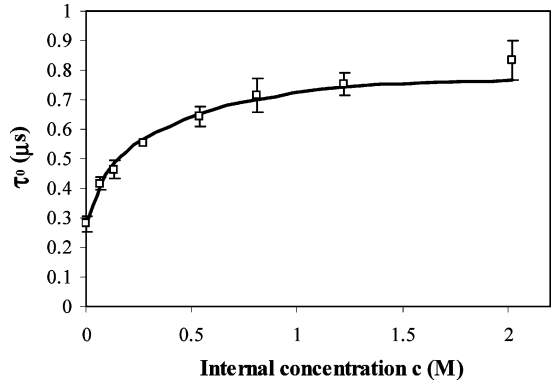

Figure 11. Dependence of gate open time on internal [Cl^-] for a neutral gate and parameter set 6.7. Results of DMC simulations (open squares with error bars) are compared with the factorized mechanism model embodied in eq 12 (solid line).

prescription: $\langle n_{cl} \rangle$ = (number of Cl^- ions in a small spatial interval of length dz centered at z)/dz, where dz was chosen to be 1 Å. Averaging over many simulation time points was performed in order to yield $\langle n_{cl} \rangle$ in units of $Å^{-1}$.] Gate open times calculated directly from DMC simulations (including all mobile ions and the gate particle) are compared with the factorized mechanism model in Figure 11. Good agreement is found.

3.5. Effect of a Negatively Charged Gate on the Gate Open Time. There is at present no consensus in the literature as to whether the glutamate residue in ClC pores is charged or not.[16,18,40,41] Thus, using our DMC model, we studied how a $-1e$ negative charge on the gate particle (where e is the proton charge) affects the gate open time. Results of DMC simulations of the system characterized by parameter set 6 are shown in Figure 12 for both the neutral and the charged gates. The single-particle PMFs (for permeating ions and for the gate particle) were assumed to be the same for both charge states of the gate. For the negatively charged gate the open time is shorter than that for the neutral one, but the saturation effect is still observed. The charge on the gate particle has two opposing influences on the gate closing rate: On one hand, this negative charge near S_{ext} increases the energy barrier for a permeating Cl^- ion to occupy the external binding site S_{ext} and thus decreases the occupation probability of S_{ext} by Cl^- ions (i.e., $f_{S_{ext}}(c)$ in eq 12). Consequently, a decrease of the gate open time is expected (cf.

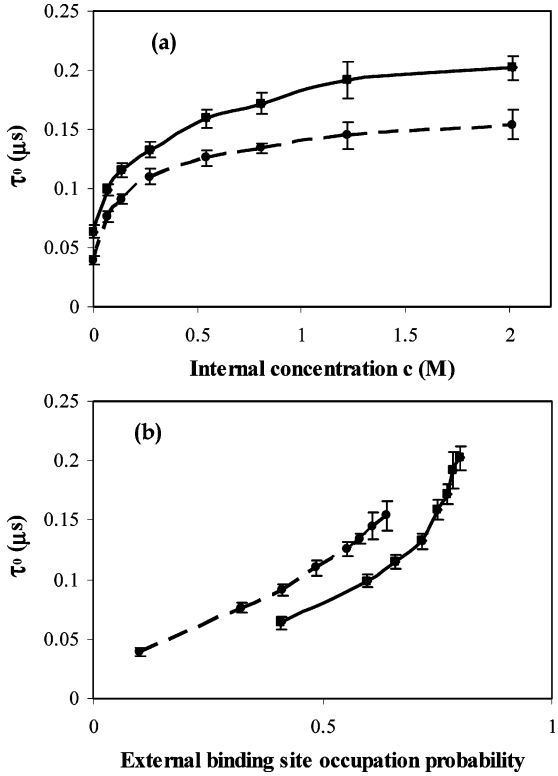

Figure 12. Dependence of the gate open time on (a) internal [Cl^-] and (b) occupation probability of Cl^- in the external binding site for both the neutral gate (squares with solid line) and the negatively charged gate (circles with dashed line) calculated for parameter set 6 (cf. Table 1) via DMC.

Figure 12a) at the same internal ion concentration. On the other hand, the repulsive electrostatic forces from permeating Cl^- ions (i.e., Cl^- ions in the external and center binding sites) make the negatively charged gate harder to close. This effect would tend to increase the gate open time. Figure 12b shows the gate open time versus the occupation probability of S_{ext} by Cl^- ion (i.e., $f_{S_{ext}}(c)$). The longer open time at the same $f_{S_{ext}}(c)$ for the charged gate is consistent with the expected consequence of electrostatic repulsion between the gate and the permeating Cl^- ions, which pushes the gate away from the S_{ext} site and thus increases the open time.

The occupation probability of S_{ext} by Cl^- ion (i.e., $f_{S_{ext}}(c)$) and the gate open time are undeniably sensitive to the value of the protein/membrane dielectric constant ϵ_p. The dielectric constant is estimated to be 2 for the membrane,[35] but there is no universal protein dielectric constant.[42] Microscopic treatments of the protein dielectric constant based on the standard Fröhlich−Kirkwood dipole moment fluctuation model and molecular dynamics simulations[35−37] suggest that the protein dielectric constant may vary between 10 and 40. Thus, to best estimate the electrostatic interactions between E166 (homologous to E148 in StClC) and permeating ions (i.e., Cl^-), we chose to employ an effective dielectric constant of $\epsilon_p = 20$ for the entire protein/membrane, cf. section 2.2 above. We note here that in several previous studies[14,27,31] a smaller ϵ_p (i.e., 2−10) was chosen to calculate the electrostatic interactions and simulate ion permeation through protein channels. Hence, we performed additional numerical simulations using two other dielectric constants, namely, $\epsilon_p = 2$ and 10, to estimate the electrostatic interactions among ions and the charged gate particle. At internal Cl^- concentration $c = 1.22$ M, $f_{S_{ext}}(c)$ was found to be 0.61, 0.44, and 0.18 for the negatively charged gate simulation systems characterized by $\epsilon_p = 20$, 10, and 2, respectively. The

corresponding gate open times were found to be 0.14, 0.1, and 0.06 μs. Lower ϵ_p leads to a larger repulsion between the gate and permeating Cl^- ions, which in turn lowers the occupancy of S_{ext} by a Cl^- ion (under the assumption that the single ion free energy is the same) and thus makes it easier for the gate to close.

4. Conclusions

We have constructed a simplified three-dimensional model channel that mimics the ClC channel in several important respects regarding geometry, energetics, and the position and function of the fast gate. Using a dynamic Monte Carlo simulation technique, we calculated the dependence of the gate open time on both internal Cl^- concentration (holding the external Cl^- concentration fixed) and external Cl^- concentration (holding the internal Cl^- concentration fixed). Our simulation results show saturation of the gate open time with the increase of the internal [Cl^-], in qualitative agreement with experiments.[6,7] External [Cl^-] concentration also regulates the fast gate, but its effect on the fast gate open time is less pronounced than that of internal [Cl^-]. The saturation behavior observed in our simulations is consistent with the foot-in-the-door mechanism and is also predicted by the simple factorized mechanism kinetic model embodied by eq 12.

The work presented here suggests future avenues of research on fast gating in ClC channels that can focus on both more and less molecular detail. In the direction of increased molecular detail, our representation of the E166 in ClC-0 channel (homologous to E148 in StClC) as a "ball on a stick" is clearly an oversimplification. The E166 glutamate side chain is a complicated and somewhat flexible molecular group. Understanding its role in gating the ClC channel would be enhanced by careful all-atom equilibrium MD simulations. Careful computations of the PMF for dihedral angles $C-C_\alpha-C_\beta-C_\gamma$ and $C_\alpha-C_\beta-C_\gamma-C_\delta$ of the E166 side chain would shed light on the energetic and mechanistic pathways by which the fast gate closes.

It would also be instructive to proceed in the direction of reduced atomic resolution, by taking advantage of the three deep minima ("binding sites") that characterize the single-particle potential seen by permeating Cl^- ions to make a discrete-state model governed by kinetic master equations that can be solved efficiently via kinetic Monte Carlo[43] or by more deterministic (matrix-based) analysis.[43,44] This reduction is motivated by the observation that even the minimalist three dimensional Brownian dynamics model developed in the present work strains available computational resources. To develop conceptual understanding of the mechanisms of fast gate-coupled ion permeation in ClC-type channels, it would be useful to have a mathematical model that enables rapid understanding of the relation between input parameters (e.g., concentration of ions in the reservoirs, depth of binding sites, relative time scale of motion of ion motion through the channel vs that of the open/close transition of the gate particle coordinate, etc.) and output (ion currents, gating times, etc.). The well-defined binding sites of the narrow channel suggest a three-site model for ions in the channel; each site can be occupied by zero or one ion. In addition, the gate particle has two stable states (open and closed) and makes transitions between these. With this effective state space, use of kinetic Monte Carlo simulation[43] or Markov chain theory[45] could be carried out with relative ease. Three-dimensional BD simulations of ion permeation coupled with motion of the additional fast gating coordinate can be run for tens of microseconds, which is not even enough time to monitor the initial closing of a channel started in the open state, let alone to follow multiple opening and closing transitions. By contrast, a discrete-state model can easily yield this information and hence the distribution of opening and closing times (from which the mean dwell time can be extracted). Of course, one needs to input state-to-state rate constants, which are difficult to obtain from first principles. However, all-atom simulations of PMFs should be able to provide effective activation barriers, etc., which will hopefully allow estimation of these critical input parameters.

Acknowledgment. We gratefully acknowledge financial support from the Army Research Office Multidisciplinary University Research Initiative (Grant No. DADD19-02-1-0227) program and the National Science Foundation (Grant No. CHE-0518044) and computation support from the Center for Molecular and Materials Simulation at the University of Pittsburgh. We would also like to thank both referees for their critical reading of this manuscript.

References and Notes

(1) Miller, C. *Philos. Trans. R. Soc. London, Ser. B* **1982**, *299*, 401−411.
(2) Dutzler, R.; Campbell, E. B.; Cadene, M.; Chait, B. T.; MacKinnon, R. *Nature* **2002**, *415*, 287−294.
(3) Dutzler, R.; Campbell, E. B.; MacKinnon, R. *Science* **2003**, *300*, 108−112.
(4) Richard, E. A.; Miller, C. *Science* **1990**, *247*, 1208−1210.
(5) Pusch, M.; Ludewig, U.; Rehfeldt, A.; Jentsch, T. J. *Nature* **1995**, *373*, 527−531.
(6) Chen, T. Y.; Miller, C. *J. Gen. Physiol.* **1996**, *108*, 237−250.
(7) Chen, T. Y.; Chen, M. F.; Lin, C. W. *J. Gen. Physiol.* **2003**, *122*, 641−651.
(8) Accardi, A.; Miller, C. *Nature* **2004**, *427*, 803−807.
(9) Chen, T. Y. *Sci. STKE* **2003**, *2003*, pe23.
(10) Estévez, R.; Schroeder, B. C.; Accardi, A.; Jentsch, T. J.; Pusch, M. *Neuron* **2003**, *38*, 47−59.
(11) Engh, A. M.; Maduke, M. *J. Gen. Physiol.* **2005**, *125*, 601−617.
(12) Lin, C.-W.; Chen, T.-Y. *J. Gen. Physiol.* **2003**, *122*, 147−159.
(13) Cohen, J.; Schulten, K. *Biophys. J.* **2004**, *86*, 836−845.
(14) Corry, B.; O'Mara, M.; Chung, S.-H. *Biophys. J.* **2004**, *86*, 846−860.
(15) Allen, T. W.; Chung, S. H. *Biochim. Biophys. Acta* **2001**, *1515*, 83−91.
(16) Bisset, D.; Corry, B.; Chung, S. H. *Biophys. J.* **2005**, *89*, 179−186.
(17) Miloshevsky, G. V.; Jordan, P. C. *Biophys. J.* **2004**, *86*, 825−835.
(18) Bostick, D. L.; Berkowitz, M. L. *Biophys. J.* **2004**, *87*, 1686−1696.
(19) Kurnikova, M. G.; Coalson, R. D.; Graf, P.; Nitzan, A. *Biophys. J.* **1999**, *76*, 642−656.
(20) Mamonov, A. B.; Coalson, R. D.; Nitzan, A.; Kurnikova, M. G. *Biophys. J.* **2003**, *84*, 3646−3661.
(21) Coalson, R. D.; Kurnikova, M. G. *IEEE Trans. Nanobiol.* **2005**, *88*, 3745−3761.
(22) Chung, S. H.; Hoyles, M.; Allen, T.; Kuyucak, S. *Biophys. J.* **1998**, *75*, 793−809.
(23) Im, W.; Seefield, S.; Roux, B. *Biophys. J.* **2000**, *79*, 788−801.
(24) O'Mara, M.; Barry, P. H.; Chung, S. H. *Proc. Natl. Acad. Sci. U.S.A.* **2003**, *100*, 4310−4315.
(25) Cheng, M. H.; Coalson, R. D. *J. Phys. Chem. B* **2005**, *109*, 488−498.
(26) Graf, P.; Nitzan, A.; Kurnikova, M. G.; Coalson, R. D. *J. Phys. Chem. B* **2000**, *104*, 12324−12338.
(27) Cheng, M. H.; Cascio, M.; Coalson, R. D. *Biophys. J.* **2005**, *89*, 1669−1680.
(28) Graf, P.; Kurnikova, M. G.; Coalson, R. D.; Nitzan, A. *J. Phys. Chem. B* **2004**, *108*, 2006−2015.
(29) Lobet, S.; Dutzler, R. *EMBO J.* **2006**, *25*, 24−33.
(30) Gervasio, F. L.; Parrinello, M.; Ceccarelli, M.; Klein, M. L. *J. Mol. Biol.* **2006**, *361*, 390−398.
(31) Faraldo-Gomez, J. D.; Roux, B. *J. Mol. Biol.* **2004**, *339*, 981−1000.
(32) Edwards, S.; Corry, B.; Kuyucak, S.; Chung, S. H. *Biophys. J.* **2002**, *83*, 1348−1360.
(33) Lide, D. R.; Kehiaian, H. V. *CRC Handbook of Thermophysical and Thermochemical Data*; CRC Press: Boca Raton, FL, 1994.
(34) Mamonov, A. B.; Kurnikova, M. G.; Coalson, R. D. *Biophys. Chem.* **2006**, *124*, 268−278.
(35) Pitera, J. W.; Falta, M.; van Gunsteren, W. F. *Biophys. J.* **2001**, *80*, 2546−2555.

(36) Simonson, T.; C. L. Brooks, I. *J. Am. Chem. Soc.* **1996**, *118*, 8452−8458.
(37) Smith, P. E.; Brunne, R. M.; Mark, A. E.; Van Gunsteren., W. F. *J. Phys. Chem.* **1993**, *97*, 2009−2014.
(38) Chandrasekhar, S. *Rev. Mod. Phys.* **1943**, *15*, 1−89.
(39) Atkins, P. W.; De Paula, J. *Physical Chemistry*, 8th ed.; Oxford University Press: Oxford, U. K., 2006.
(40) Yin, J.; Kuang, J. Z.; Mahankali, U.; Beck, T. L. *Proteins* **2004**, *57*, 414−421.
(41) Chen, M. F.; Chen, T. Y. *J. Gen. Physiol.* **2001**, *118*, 23−32.
(42) Schutz, C. N.; Warshel, A. *Proteins* **2001**, *44*, 400−417.
(43) Lu, D.; Grayson, P.; Schulten, K. *Biophys. J.* **2003**, *85*, 2977−2987.
(44) Elston, T. C. *J. Math. Biol.* **2000**, *41*, 189−206.
(45) Deng, Y.; Peng, S.; Qian, M.; Feng, J. *J. Phys. A* **2003**, *36*, 1195−1212.
(46) Robinson, R. A.; Stokes, R. H. *Electrolyte Solutions*, 2nd ed.; Butterworths: London, U. K., 1965.